Probing the Evolution of the Electron Spin Wave Function of the Nitrogen-Vacancy Center in Diamond via Pressure Tuning

Kin On Ho,[1,‡] Man Yin Leung,[2,‡] P. Reddy,[3,‡] Jianyu Xie,[1,‡] King Cho Wong,[1,‡] Yaxin Jiang,[1]
Wei Zhang,[1] King Yau Yip,[1] Wai Kuen Leung,[2] Yiu Yung Pang,[1] King Yiu Yu,[1]
Swee K. Goh,[1,4] M.W. Doherty,[3,*] and Sen Yang[1,2,†]

[1]*Department of Physics, The Chinese University of Hong Kong, Shatin, New Territories, Hong Kong, China*

[2]*Department of Physics and the IAS Centre for Quantum Technologies, The Hong Kong University of Science and Technology, Clear Water Bay, Kowloon, Hong Kong, China*

[3]*Laser Physics Centre, Research School of Physics and Engineering, Australian National University, 2601, Australia*

[4]*Shenzhen Research Institute, The Chinese University of Hong Kong, Shatin, New Territories, Hong Kong, China*

Understanding the profile of a qubit's wave function is key to its quantum applications. Unlike conducting systems, where a scanning tunneling microscope can be used to probe the electron distribution, there is no direct method for solid-state-defect-based qubits in wide-band-gap semiconductors. In this work, we use pressure as a tuning method and a nuclear spin as an atomic scale probe to monitor the hyperfine structure of negatively charged nitrogen-vacancy (N-V) centers in diamonds under pressure. We present a detailed study on the nearest-neighbor ^{13}C hyperfine splitting in the optically detected magnetic resonance spectrum of N-V centers at different pressures. By examining the ^{13}C hyperfine interaction upon pressurizing, we show that the N-V hyperfine parameters have prominent changes, resulting in an increase in the N-V electron spin density and rehybridization from sp^3 to sp^2 bonds. The *ab initio* calculations of strain dependence of the N-V center's hyperfine levels are done independently. The theoretical results qualitatively agree well with experimental data without introducing any fitting parameters. Furthermore, this method can be adopted to probe the evolution of wave function in other defect systems. This potential capability could play a role in developing magnetometry and quantum information processing using the defect centers.

I. INTRODUCTION

The study of a qubit's wave function is the heart of solving quantum systems, yet the theoretical computation of such wave functions is often demanding. Unlike conducting systems whose wave functions can be practically probed by a scanning tunneling microscope (STM), the wave functions of point defects in wide-band-gap semiconductors cannot be directly measured, since the defects are highly confined in the insulating host material. Hence, understanding the wave functions of such defects is also experimentally challenging. It was proposed that the responses of a solid-state defect's wave function to thermal expansion or mechanical stress can be studied via measuring the hyperfine interactions between the defect and its nearby nuclear spins [1–7]. Thermal

*marcus.doherty@anu.edu.au

†phsyang@ust.hk

‡These authors contributed equally to this work.

expansion is typically a weak effect and noticeable changes have not been observed until recently [3–7]. On the other hand, stress is a much stronger lattice tuner than temperature. In this work, we demonstrate the measurement of stress-dependent hyperfine interaction in a point defect system for the first time and an accord between theoretical and experimental results without introducing any fitting parameters.

The point defect we investigate is the negatively charged nitrogen-vacancy (N-V) center in diamond, a color center consisting of a substitutional nitrogen atom and an adjacent carbon vacancy. The N-V center has unprecedented potential in the fields of quantum metrology [2,8–20], information [21–23], and communication [24–26]. In particular, it is a promising sensor with superior spatial resolution and sensitivity, and its electron spin resonance (ESR) can be readily measured via the optically detected magnetic resonance (ODMR) method due to the spin-state-dependent fluorescence rate. The transitions between the triplet ground states $|m_s\rangle = |0\rangle$ and

$|m_s\rangle = |\pm 1\rangle$ are found to be approximately 2870 MHz at ambient conditions [27]. Several pioneer works have revealed the stress susceptibility of the N-*V* center [28–38], but the fundamental origin of this response is not completely clear yet, for instance, how the spin density and hybridization ratio of the N-*V* center's orbitals may change under stress. Precision quantum sensing and high-fidelity quantum information processing operations require well-characterized susceptibilities and an accurate understanding of the physical origin, and stress is one of the least explored parameters.

To probe the evolution of electron spin wave function of a N-*V* center, one has to use the nearest-neighbor nuclear spins to have enough overlap with the wave function of the N-*V* unpaired electrons. In a natural diamond, a small natural abundance (1.1%) of carbon atoms exists as ^{13}C with nuclear spin $I = 1/2$. If one of the nearest carbon atoms is ^{13}C instead of ^{12}C, the N-*V* electron spin couples with it via strong magnetic dipole-dipole interaction and Fermi contact interaction [39], and the hyperfine coupling is about 127 MHz at ambient conditions [3,40–45]. This is 2 orders of magnitude stronger than another common hyperfine coupling with the nearest ^{14}N nuclear spin, which is around 2 MHz. The nearest ^{13}C neighbors can thus be an ideal probe for the change in the N-*V* center wave function under stress.

Upon applying hydrostatic pressure, we expect the nuclei surrounding the N-*V* center to change their positions significantly [1,2], so the N-*V* electron spin density and orbital hybridization of the unpaired N-*V* spin would change accordingly [3]. These wave-function responses are encrypted in the pressure-dependent ^{13}C hyperfine parameters of the N-*V* center. In this work, we first outline the theory behind the ^{13}C hyperfine interaction and the N-*V* electron spin wave function. We then experimentally study the resonances in the ODMR spectrum associated with the nearest-neighbor ^{13}C hyperfine interaction under hydrostatic pressure. This is an exciting attempt to measure the changes in the atomic level of the N-*V* center via external perturbations.

II. MODEL

Using the basis defined as $|m_s, m_I\rangle = \{|1, 1/2\rangle, |1, -1/2\rangle, |0, 1/2\rangle, |0, -1/2\rangle, |-1, 1/2\rangle, |-1, -1/2\rangle\}$, the N-*V*+^{13}C Hamiltonian is given by [42]

$$H = \begin{pmatrix} a + \frac{D}{3} & \sqrt{2}d^* & d^* & c^* & 0 & 0 \\ \sqrt{2}d & \frac{D}{3} - a & b & -d^* & 0 & 0 \\ d & b & -\frac{2D}{3} & 0 & d^* & c^* \\ c & -d & 0 & -\frac{2D}{3} & b & -d^* \\ 0 & 0 & d & b & \frac{D}{3} - a & -\sqrt{2}d^* \\ 0 & 0 & c & -d & -\sqrt{2}d & a + \frac{D}{3} \end{pmatrix}.$$
(1)

In a coordinate system where the N-*V* and ^{13}C reference frames coincide in the *x* axes [46], the matrix elements can be expressed as [47]

$$a = \frac{A_{zz}}{2}, b = \frac{A_{xx} + A_{yy}}{2\sqrt{2}}, c = \frac{A_{xx} - A_{yy}}{2\sqrt{2}}, d = i\frac{A_{yz}}{2\sqrt{2}}. \quad (2)$$

$$\begin{aligned} A_{xx} &= A_\perp, \theta = 109.47°, \\ A_{yy} &= A_\parallel \sin^2\theta + A_\perp \cos^2\theta, \\ A_{zz} &= A_\parallel \cos^2\theta + A_\perp \sin^2\theta, \\ A_{yz} &= A_{zy} = (A_\parallel - A_\perp)\sin\theta\cos\theta. \end{aligned} \quad (3)$$

Effectively, there are only three variables: $A_\parallel$, $A_\perp$, and D. This 6×6 matrix has three doubly degenerate roots, which can be analytically solved by the Cardano formulas (details in Refs. [42,47]). The transitions from these three N-*V*+^{13}C eigenvalues (energy levels) can be readily measured from the dips in our ODMR spectra. The calculations can be generalized to the cases under pressure, implying that we can solve $A_\parallel(P)$ and $A_\perp(P)$ from $\Delta_{hf}(P)$, $\delta_{hf}(P)$, and $D(P)$ under pressure P measured by N-*V* centers ($dD/dP = 1.49$ MHz/kbar [9]).

Using hyperfine parameters $A_\parallel(P)$ and $A_\perp(P)$ determined from ODMR parameters $\Delta_{hf}(P)$ and $\delta_{hf}(P)$, we can compute the Fermi contact term $f(P)$ and the dipole term $d(P)$, thus the electron spin density $\eta(P)$ and the hybridization of p orbitals $|c_p(P)|^2$. They are related as [3,39,48,49]

$$A_\parallel(P) = f(P) + 2d(P), \quad (4)$$

$$A_\perp(P) = f(P) - d(P). \quad (5)$$

$$f(P) = 3777 \times \left(1 - |c_p(P)|^2\right)\eta(P)\ \text{MHz}, \quad (6)$$

$$d(P) = 107.4 \times |c_p(P)|^2\eta(P)\ \text{MHz}, \quad (7)$$

where η is the electron spin density at the nucleus and $|c_p|^2$ is the hybridization of p orbitals. These relations show that measuring $A_\parallel$ and $A_\perp$ to obtain f and d allows for the determination of the pressure-dependent changes in the electron spin density η and the N-*V* orbital hybridization $|c_s|^2/|c_p|^2$, where $|c_s|^2$ is the hybridization of s orbitals. Here, it is assumed that the contribution to the total molecular orbitals (MOs) from an atomic orbital at the nuclear spin is a hybrid orbital ψ, which is a linear combination of s (ϕ_s) and p orbitals (ϕ_p) [39], and ψ satisfies

$$\begin{aligned} \psi &= c_s\phi_s + c_p\phi_p, \\ 1 &= |c_s|^2 + |c_p|^2. \end{aligned} \quad (8)$$

III. DFT CALCULATION

Independent *ab initio* calculations are performed to derive the N-V+^{13}C hyperfine structure under applied stress for comparison to experimental findings [47]. These calculations are performed using the Vienna *ab initio* simulation package (VASP). We study a 512 atom supercell containing a N-V center with a ^{13}C nearest neighbor. All calculations use a 600 eV plane-wave cutoff energy and the Perdew-Burke-Ernzerhof (PBE) functional. The hyperfine interaction is evaluated in the N-V ground state using the in-built hyperfine routine from VASP.

We calculate zero-field hyperfine energies that are in agreement with the accepted theoretical values: $\Delta_{hf}(0) = 127.604$ MHz and $\delta_{hf}(0) = 2876.86$ MHz. The dependence of Δ_{hf} on stress is evaluated as follows:

$$\frac{\partial \Delta_{hf}}{\partial \sigma_{ij}} = \begin{bmatrix} 0.0487 & 0.0067 & -0.0063 \\ 0.0067 & 0.0357 & 0.0003 \\ -0.0063 & 0.0003 & 0.0342 \end{bmatrix} \text{MHz/kbar},$$

$$(9)$$

where σ_{ij} are the stress-tensor components and i,j index the coordinates $(x,y,z) = ([100],[010],[001])$ in crystallographic notation. Our calculations also find that the components of the δ_{hf} hyperfine-stress interaction are on the order of 0.1 kHz/kbar. Notably, this is 4 orders of magnitude smaller than the spin-spin dependence on strain (which is on the order of 1 MHz/kbar).

To compare with experiment results, we estimate the hyperfine structure under purely hydrostatic pressures. The dependence of Δ_{hf} with hydrostatic pressure is calculated as follows:

$$\frac{\partial \Delta_{hf}}{\partial P} = \left(\frac{\partial \Delta_{hf}}{\partial \sigma_{xx}} + \frac{\partial \Delta_{hf}}{\partial \sigma_{yy}} + \frac{\partial \Delta_{hf}}{\partial \sigma_{zz}} \right)/3$$

$$= 0.1186/3 \approx 0.039\,53 \text{ MHz/kbar}. \quad (10)$$

In the discussion below, the theoretical ambient values are always taken as $\Delta_{hf}(0) = 127.604$ MHz and $\delta_{hf}(0) = 2876.86$ MHz. The dependence of δ_{hf} on hydrostatic pressure is approximated as the spin-stress interaction $\partial D/\partial P = 1.49$ MHz/kbar [9]. Combining these results, the hyperfine energy levels are approximated by the following expressions:

$$\Delta_{hf}(P) \approx \Delta_{hf}(0) + \frac{\partial \Delta_{hf}}{\partial P}P$$

$$= 127.604 + 0.039\,53P \text{ MHz}, \quad (11)$$

$$\delta_{hf}(P) \approx \delta_{hf}(0) + \frac{\partial D}{\partial P}P$$

$$= 2876.86 + 1.49P \text{ MHz}. \quad (12)$$

IV. EXPERIMENTS

The illustration of our high-pressure device is shown in Fig. 1(a), where a diamond anvil cell (DAC) is harnessed to pressurize some 1-μm diamond particles (NDs) dropcasted on one of the anvil culets. To measure spin resonance at high pressures, a 150-μm-diameter Ω-shaped gold microstructure is fabricated on one of the anvils to have uniform and reliable microwave (MW) transmission [50]. To ensure an excellent hydrostatic condition up to approximately 100 kbar at room temperature, 4:1 methanol:ethanol mixture is used as the pressure medium [51–54]. The pressure is calibrated by individual NDs
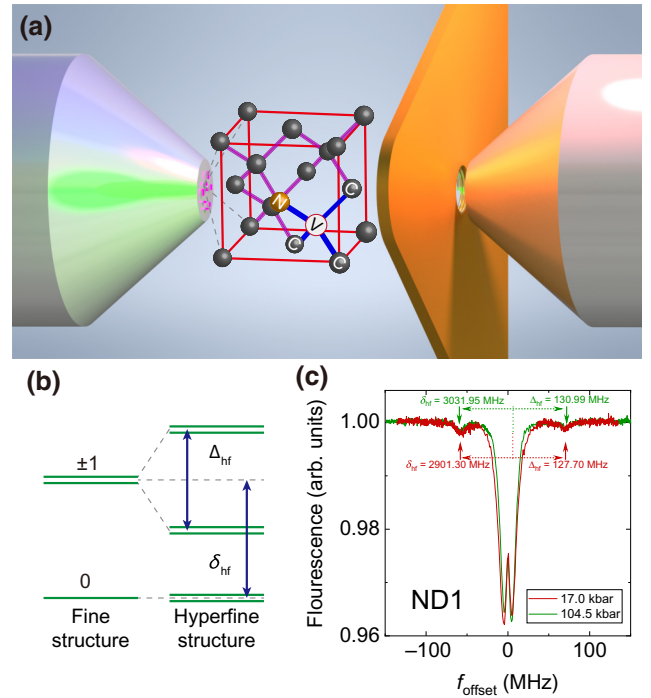

FIG. 1. (a) Illustration of our DAC. 1-μm NDs are dropcasted onto one of the anvil culets. 4:1 methanol:ethanol mixture is used as the pressure medium that is confined by a metallic gasket, while two aligned diamond anvils are used for generating pressure. The central hole of the gasket had a diameter of 300 μm. A 150-μm-diameter Ω-shaped gold microstructure is used as a MW antenna for ODMR measurements. (b) The energy levels of the hyperfine structures. There are two ^{13}C ODMR parameters Δ_{hf} and δ_{hf}, which correspond to the separation and center of the two hyperfine resonances, respectively. (c) The ODMR spectra of the same ND at 17.0 and 104.5 kbar. The f_{offest} is defined as the difference from the center frequency D. The pressure-induced changes in hyperfine resonances in the ODMR spectrum upon pressure change could be directly observed. It is obvious that the ^{13}C hyperfine resonances have relatively broad linewidths and low contrasts compared to the center resonances. The pressure is determined by the center frequency of the corresponding ODMR spectrum [9].

using $dD/dP = 1.49$ MHz/kbar [9]. Details are in the Appendix.

V. RESULTS

Figure 1(b) shows the energy levels of the ^{13}C hyperfine structure. From the ODMR spectrum of N-V centers, two parameters could be read out: Δ_{hf} and δ_{hf}, which correspond to the separation and center of the two ^{13}C ODMR resonances, respectively. An example of ODMR spectrum of a 1-μm ND at ambient conditions is shown in the Appendix, and the corresponding hyperfine parameters are $\Delta_{hf}(0) = 127.62 \pm 0.54$ MHz and $\delta_{hf}(0) = 2876.95 \pm 0.38$ MHz. These values are in excellent agreement to the previous studies [3,40–45]. The small discrepancy may be due to internal strain and different charge environments in the ^{13}C sample. Therefore, we perform averages over NDs in our data analysis to have statistical results. On the other hand, as the contrast of ^{13}C ODMR resonances is relatively weak, peak fitting may contribute a small offset to the result (see Appendix). The ODMR spectra at 17.0 and 104.5 kbar of the same ND are shown in Fig. 1(c). The changes in hyperfine resonances in the ODMR spectrum upon pressure change could be directly observed without any peak-fit processing. To retain high spectral resolution while minimizing measurement time, we implement a nonuniform ODMR measurement to capture the changes. We use a smaller MW frequency step in the hyperfine resonance regions while a larger MW frequency step in the central region. The pressure is determined by the center frequency D of the corresponding ODMR spectrum [9].

The experimental data of $\Delta_{hf}(P)$ and $\delta_{hf}(P)$ at different pressures are plotted in Fig. 2. Three NDs are tracked. We try three different ways to process the data of $\Delta_{hf}(P)$ and $\delta_{hf}(P)$: (i) perform a linear fit for each of the three NDs; (ii) take the average of the three then perform a linear fit (AVG); and (iii) take the average after performing individual linear fits (AVG2). The changes in Δ_{hf} and δ_{hf} upon

TABLE I. Data summary of the ^{13}C ODMR parameters $\Delta_{hf}(P)$ and $\delta_{hf}(P)$. All values are in MHz unit. Our data are in great agreement with the theory.

Label	$\Delta_{hf}(0)$	$d\Delta_{hf}/dP$	$\delta_{hf}(0)$	$d\delta_{hf}/dP$
ND1	126.85	0.033	2876.17	1.492
ND2	128.25	0.033	2874.96	1.500
ND3	128.27	0.036	2878.41	1.463
AVG	127.69	0.035	2877.05	1.482
AVG2	127.79	0.034	2876.51	1.485
Theory	127.604	0.039 53	2876.86	1.49

pressure change are pronounced. When pressure increases, the ^{13}C ODMR parameters Δ_{hf} and δ_{hf} gradually increase. For Δ_{hf}, the data are slightly scattered among different NDs but the same increasing behavior is noted. The discrepancy is from the local charge environment and lattice strain, as well as tiny strain perturbation projected to the N-V local frame. For δ_{hf}, the data points fall nicely on the same linear line. Note that the pressure dependence of $\delta_{hf}(P)$ is dominated by the spin-spin dependence (dD/dP), hence the discrepancy in $\delta_{hf}(P)$ is much smaller compared to $\Delta_{hf}(P)$. These results are summarized in Table I and they are in great agreement with the theoretical calculation. Figure 2 is strong evidence showing that the hyperfine parameters $A_\parallel$ and $A_\perp$ change under pressure. Additional data are shown within the Supplemental Material [47].

Our results reveal a prominent change in the hyperfine parameters $A_\parallel$ and $A_\perp$, thus suggesting a possible variation in the N-V electron spin wave function upon applying pressure. To quantify the changes in the N-V electron spin density and orbital hybridization, the ^{13}C ODMR parameters Δ_{hf} and δ_{hf} are first converted to hyperfine parameters $A_\parallel$ and $A_\perp$, then further to the Fermi contact f and dipole term d, and finally, to the orbital hybridization $|c_s|^2/|c_p|^2$ and electron spin density η. The derived results are shown in Fig. 3, which indicates that under applied hydrostatic pressure the electron density increases while the defect orbitals become more s-like and less p-like. Applying a qualitative model of the defect, we expect the orbitals to become more localized to the atoms around the vacancy. This is because pressure reduces the size of lattice unit cell, resulting in a deepening of the potential well of the vacancy and hence an increased attraction of electron density. We also expect that the N-V center self-distorts away from a tetrahedral configuration under pressure. As a result, the bonds between the nearest neighbor and next-to-nearest carbon atoms become more like sp^2 bonds and less like sp^3 bonds. This is consistent with the decrease in the p-orbital contribution to the bonds, $|c_p|^2$. Figure 4 illustrates the lattice distortion under pressure, which gives rise to changes in orbital hybridization of the unpaired N-V spin and electron spin density at the location of the nuclear spin.
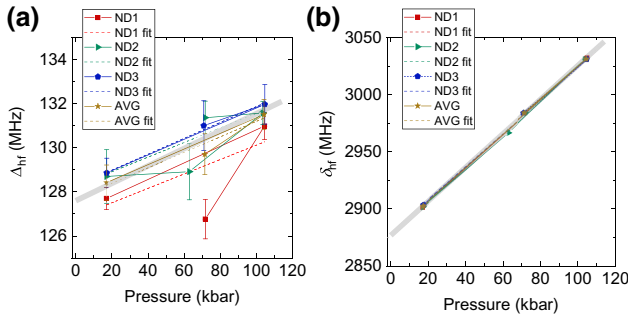
FIG. 2. Plots of ^{13}C ODMR parameters (a) $\Delta_{hf}(P)$ and (b) $\delta_{hf}(P)$ against pressure. Three NDs are tracked. The joining lines signify the data measurement sequence. The changes in Δ_{hf} and δ_{hf} with pressure are pronounced. The linear fits are the dash lines. The light gray line in the background is the theory result.
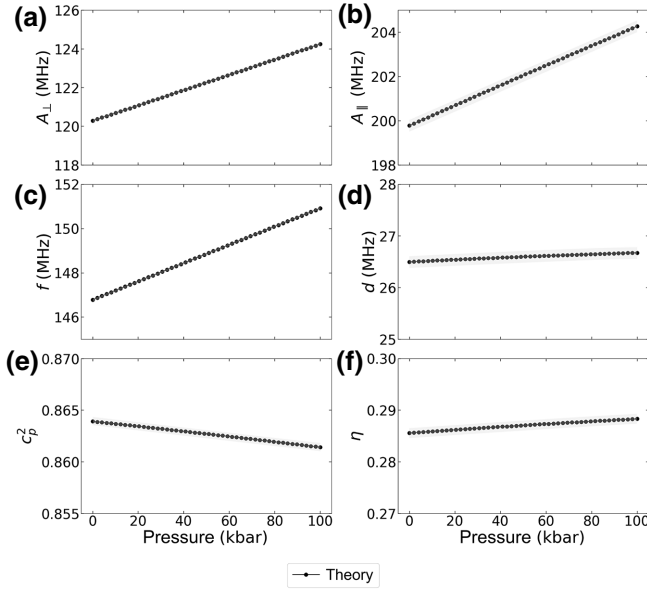
FIG. 3. Derived results of (a) hyperfine constant $A_\perp$, (b) hyperfine constant $A_\parallel$, (c) Fermi contact term f, (d) dipole term d, (e) hybridization of the p orbitals $|c_p|^2$, and (f) electron spin density η. The black markers are derived purely from theoretical values. The electron density η increases while the p-orbital contribution $|c_p|^2$ decreases, both slightly. The green error bound is from the maximum uncertainty of the theoretical resolution of 0.1 kHz/kbar. This theoretical resolution is the smallest energy difference resolvable in our calculations. It mainly affects the terms $d\delta_{hf}/dP$ since the neglected hyperfine-stress interaction in δ_{hf} is of the same order. Furthermore, the term $d\delta_{hf}/dP$ is shown to be the most sensitive input parameter that impacts the derived results [47]. Note that the theoretical resolution of 0.1 kHz/kbar is much better than the test case of, yet still merely, 0.1% difference (around 1 kHz/kbar).

VI. DISCUSSIONS

The nonlinearity nature of solving the Hamiltonian backwards from Δ_{hf} and δ_{hf} to $A_\parallel$ and $A_\perp$ leads to sensitive dependence on certain parameters. Although our measurement data match the theoretical values pretty well, small differences are severely amplified by the nonlinear equations. We test all four ^{13}C ODMR parameters [slopes and intercepts of $\Delta_{hf}(P)$ and $\delta_{hf}(P)$] and study how sensitive are the six derived quantities in Fig. 3 to them. The analysis is summarized in Ref. [47]. Surprisingly, changing $d\Delta_{hf}/dP$ does not alter the calculations by much, even changing $\Delta_{hf}(0)$ seems to only offset the calculations by a little amount. However, $d\delta_{hf}/dP$ affects the calculations significantly. Merely changing $d\delta_{hf}/dP$ by 0.1% (around 1 kHz/kbar) can significantly modify the result, even giving different signs of the slopes of the electron spin density $\eta(P)$ and p-orbital hybridization $|c_p(P)|^2$. The components of the δ_{hf} hyperfine-stress interaction are on the order of 0.1 kHz/kbar as stated in the theory section, and hence a
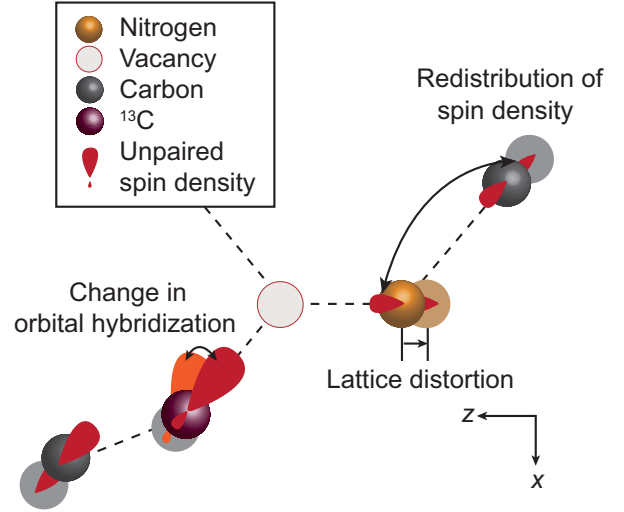

FIG. 4. Schematic of lattice distortion and the consequent redistribution of spin density between atoms and rehybridization of the atomic orbitals. The arrows indicate the displacements of atoms for increasing pressure. The axes (X, Z) correspond to the crystallographic coordinate system.

seemingly small change of 1 kHz/kbar in $d\delta_{hf}/dP$ actually matters. The change in $\delta_{hf}(0)$ also offsets the values significantly, but the trends are similar.

In principle, the experimental resolution can be improved by ENDOR Raman-heterodyne [55] or pulsed NMR measurements. However, the low abundance of ^{13}C limits the sensitivity. By using ^{13}C-enriched samples, one can reach higher accuracy and the problem of low ^{13}C concentration may not be a limitation in other defect systems. Furthermore, we are using a commercial ND product, while further work will require custom specifications to enhance the resolution.

In future work, HSE calculations can be conducted to further reveal the localization of electronic states and hyperfine parameters [56,57]. The accuracy of PBE N-V hyperfine is due to a fortuitous cancellation of two main effects. First, neglecting the spin polarization of the core electrons results in a systematic overestimation of the hyperfine interaction. Second, the spin density calculated with PBE is less localized, resulting in a systematic underestimation of the hyperfine interaction. Previous work has identified systematic overestimation and underestimation cancel to fortuitously give the near-exact agreement seen in PBE. While this fortuitous cancellation may persist under applied strain, the discrepancy will be bounded by about 20%.

Note that the thermal and pressure effects are similar but not identical. While pressure and temperature can change lattice constant, temperature also changes the distribution of phonon modes, hence changing the optical and spin properties. From this perspective, pressure tuning is a cleaner approach to have an isolated effect on the

parameters for systematic studies. Actually, by combing both approaches, i.e., scanning temperature in this pressure method, one may decouple the thermal and phonon effect. Moreover, a pressure cell is a small portable device and is more robust than a cooler or heater. Meanwhile, the pressure tuning method is orders of magnitude stronger than the thermal one, providing a much wider scanning range of lattice changes.

In summary, we reveal the pressure dependence of the ^{13}C hyperfine structure. In particular, we focus on the hyperfine interaction between the N-V electron spin and the ^{13}C nuclear spin, which leads to the detection of the N-V center electron spin density and orbitals. Under applied hydrostatic pressure, the electron spin density η increases while the defect orbitals become more like sp^2 bonds and less like sp^3 bonds. These can be explained by the reduction of the cell size and the self-distortion of the N-V center. By using pressure tuning and ^{13}C nuclear spins as a probe, we demonstrate that one can investigate the wave functions of deep defects in semiconductors. This method can be adopted to study similar defect systems with hyperfine structure. Hence, we can adopt this process to understand and optimize the quantum sensing and computing applications of a wide array of deep defects in semiconductors.

APPENDIX A: HIGH-PRESSURE DEVICE

The DAC consists of two anvils pressing against each other with a metallic gasket in between. A hole of 300 μm is drilled in the middle of the gasket to create a pressure chamber in which we place the diamond sample. We investigate 1-μm NDs with a nitrogen concentration of 3 ppm. The NDs are dropcasted on one of the two anvil culets. The chamber is then filled with a pressure medium for effective pressure transfer from the anvils into the chamber. Spin resonance measurements are not trivial at high pressures, since it requires a robust and delicate MW structure that can survive in a high-stress environment. Deterioration of the pressure system and MW heating should also be avoided to prevent undesired changes in N-V centers. A 150-μm-diameter Ω-shaped gold microstructure is fabricated on one of the anvils to have uniform MW transmission [50]. To ensure an excellent hydrostatic condition, 4:1 methanol:ethanol mixture is used as the pressure medium (see below).

APPENDIX B: HYDROSTATICITY OF 4:1 METHANOL:ETHANOL MIXTURE

4:1 methanol:ethanol mixture is one of the best liquid-type pressure media. Although gas-type media can provide an even better pressure environment, they are not trivial to handle and require gas-loading equipment. In practice, the 4:1 methanol:ethanol mixture stays in excellent hydrostatic conditions up to approximately 100 kbar at room temperature [51–54]. Above the glass-transition pressure P_g, this mixture enters its glassy phase and forms an amorphous solid. Under this circumstance, a pressure gradient can be easily built up to terminate the hydrostatic pressure condition. To show the hydrostatic condition of our experiments, we plot in Fig. 5 the average transverse zero-field splitting E (splitting of the center resonances in ODMR spectra equals 2E) and the SD of the center frequency D as functions of the average pressure. The pressure is calibrated by individual NDs using $dD/dP = 1.49$ MHz/kbar [9]. In particular, SD analysis is relevant in different kinds of pressure media [9,54]. The presence of a nonhydrostatic pressure can induce sharp changes in ODMR spectra as well as the SD of D measured among different NDs in the medium. We show that although the pressure gradient builds up before the expected P_g, the gradient is rather negligible (only a tiny fraction of the average pressure even at approximately equal to 100 kbar). We can therefore infer from our observed invariance in average E and SD that the applied pressure is highly hydrostatic within our pressure range up to approximately 100 kbar, meaning that the hydrostatic pressure approximation works well in our experiment.

APPENDIX C: ANALYZING THE ODMR SPECTRA

The pressure-driven changes in hyperfine resonances in the ODMR spectrum could be directly observed without
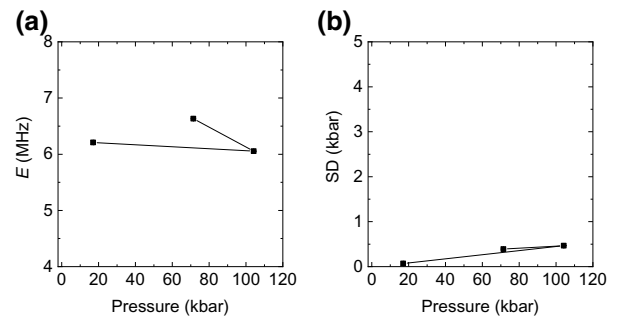
FIG. 5. (a) The average E and (b) the SD of the center frequency D verse the average pressure measured by NDs ($dD/dP = 1.49$ MHz/kbar [9]). The joining lines signify the data measurement sequence. From the insignificant variations in these quantities under applied pressure, we conclude that the mixture is in excellent hydrostatic condition within our pressure range, meaning that the hydrostatic pressure approximation works well.

any peak fitting, as shown in Fig. 1(c). However, there are two main concerns about analyzing ODMR spectra. Firstly, the hyperfine resonances from ^{13}C have broad linewidths (approximately 10 MHz) and low contrasts ($<$ 0.5%). As a result, the fitting of the hyperfine resonances is greatly affected by noise and fitting parameters. Secondly, due to intrinsic large strain and local charge environment in the NDs, the N-V center resonance peak is relatively broad and also splits into two resonances. The broadening is further intensified by MW power. As the ^{13}C hyperfine peaks lie on the tails of the center resonance peaks, the broad center resonance peaks may mask the ^{13}C peaks a bit. This unavoidably affects the fitting on the ^{13}C hyperfine resonances. As a result, the fitting method for the hyperfine resonances plays an essential role in determining the ^{13}C ODMR parameters. To deal with this problem, we try various fitting procedures, for example, we try different fitting functions like Lorentzian and Gaussian, a different number of fitting peaks, and ignoring the center resonances to fit the hyperfine resonances. Nevertheless, we do not find the most suitable and convincing fitting procedures to precisely extract the ODMR parameters.

In the end, we decide to use the most straightforward way to process—use four Lorentzians to directly fit all our measured ODMR spectra. In some cases, we find that the baseline (y_0) is needed to be fixed, but for consistency, we fix all the baselines in our analysis. This may be because the baseline does not extend wide enough in our measured spectra and the fitting program mistakes a higher value for the baseline, which is obviously incorrect. To have the same criterion for the baseline, we first apply two Lorentzians to fit the N-V center resonances, and the corresponding baseline is extracted for the subsequent four-Lorentzian fitting. One advantage of four-Lorentzian fitting is that the absolute values of Δ_{hf} at very low pressure appear to be closer to the theoretical values at ambient pressure. Although the data we report are still slightly different from the ideal theoretical values, as long as we stick to the same fitting procedure, this offset will be approximately the same and the changes in hyperfine structure are still meaningful. An example of the fitting at ambient pressure is shown in Fig. 6.

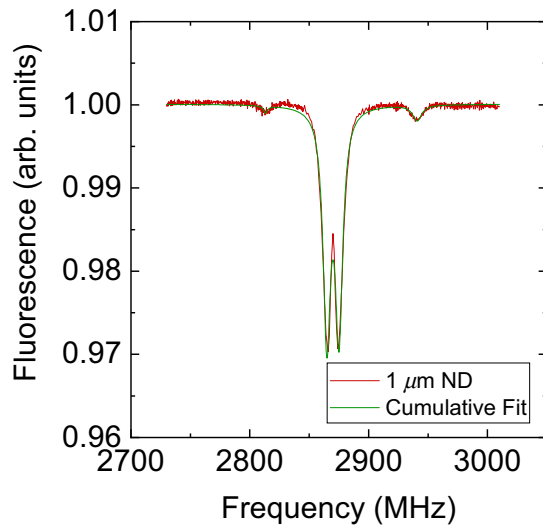

FIG. 6. An example of the fitting at ambient pressure. Red line is the raw data and green line is the cumulative fit of the four-Lorentzian peaks.

[1] M. S. J. Barson, P. Peddibhotla, P. Ovartchaiyapong, K. Ganesan, R. L. Taylor, M. Gebert, Z. Mielens, B. Koslowski, D. A. Simpson, L. P. McGuinness, J. McCallum, S. Prawer, S. Onoda, T. Ohshima, A. C. Bleszynski Jayich, F. Jelezko, N. B. Manson, and M. W. Doherty, Nanomechanical sensing using spins in diamond, Nano Lett. **17**, 1496 (2017), pMID: 28146361.

[2] M. W. Doherty, V. V. Struzhkin, D. A. Simpson, L. P. McGuinness, Y. Meng, A. Stacey, T. J. Karle, R. J. Hemley, N. B. Manson, L. C. L. Hollenberg, and S. Prawer, Electronic Properties and Metrology Applications of the Diamond NV$^-$ Center Under Pressure, Phys. Rev. Lett. **112**, 047601 (2014).

[3] M. S. J. Barson, P. Reddy, S. Yang, N. B. Manson, J. Wrachtrup, and M. W. Doherty, Temperature dependence of the ^{13}C hyperfine structure of the negatively charged nitrogen-vacancy center in diamond, Phys. Rev. B **99**, 094101 (2019).

[4] V. V. Soshenko, V. V. Vorobyov, S. V. Bolshedvorskii, O. Rubinas, I. Cojocaru, B. Kudlatsky, A. I. Zeleneev, V. N. Sorokin, A. N. Smolyaninov, and A. V. Akimov, Temperature drift rate for nuclear terms of the NV-center ground-state Hamiltonian, Phys. Rev. B **102**, 125133 (2020).

[5] A. Jarmola, I. Fescenko, V. M. Acosta, M. W. Doherty, F. K. Fatemi, T. Ivanov, D. Budker, and V. S. Malinovsky, Robust optical readout and characterization of nuclear spin transitions in nitrogen-vacancy ensembles in diamond, Phys. Rev. Res. **2**, 023094 (2020).

[6] G. Wang, A. R. Barr, H. Tang, M. Chen, C. Li, H. Xu, J. Li, and P. Cappellaro, Characterizing temperature and strain variations with qubit ensembles for their robust coherence protection (2022).

[7] H. Tang, A. R. Barr, G. Wang, P. Cappellaro, and J. Li, First-principles calculation of the temperature-dependent transition energies in spin defects (2022).

[8] K. Y. Yip, K. O. Ho, K. Y. Yu, Y. Chen, W. Zhang, S. Kasahara, Y. Mizukami, T. Shibauchi, Y. Matsuda, S. K. Goh, and S. Yang, Measuring magnetic field texture in correlated electron systems under extreme conditions, Science **366**, 1355 (2019).

[9] K. O. Ho, M. Y. Leung, Y. Jiang, K. P. Ao, W. Zhang, K. Y. Yip, Y. Y. Pang, K. C. Wong, S. K. Goh, and S. Yang, Probing Local Pressure Environment in Anvil Cells with Nitrogen-Vacancy (N-V^-) Centers in Diamond, Phys. Rev. Appl. **13**, 024041 (2020).

[10] M. Lesik, T. Plisson, L. Toraille, J. Renaud, F. Occelli, M. Schmidt, O. Salord, A. Delobbe, T. Debuisschert, L. Rondin, P. Loubeyre, and J.-F. Roch, Magnetic

measurements on micrometer-sized samples under high pressure using designed NV centers, Science **366,** 1359 (2019).

[11] S. Hsieh, P. Bhattacharyya, C. Zu, T. Mittiga, T. J. Smart, F. Machado, B. Kobrin, T. O. Höhn, N. Z. Rui, M. Kamrani, S. Chatterjee, S. Choi, M. Zaletel, V. V. Struzhkin, J. E. Moore, V. I. Levitas, R. Jeanloz, and N. Y. Yao, Imaging stress and magnetism at high pressures using a nanoscale quantum sensor, Science **366,** 1349 (2019).

[12] G. Kucsko, P. C. Maurer, N. Y. Yao, M. Kubo, H. J. Noh, P. K. Lo, H. Park, and M. D. Lukin, Nanometre-scale thermometry in a living cell, Nature **500,** 54 (2013).

[13] F. Dolde, H. Fedder, M. W. Doherty, T. Nöbauer, F. Rempp, G. Balasubramanian, T. Wolf, F. Reinhard, L. C. L. Hollenberg, F. Jelezko, and J. Wrachtrup, Electric-field sensing using single diamond spins, Nat. Phys. **7,** 459 (2011).

[14] N. M. Nusran, K. R. Joshi, K. Cho, M. A. Tanatar, W. R. Meier, S. L. Bud'ko, P. C. Canfield, Y. Liu, T. A. Lograsso, and R. Prozorov, Spatially-resolved study of the Meissner effect in superconductors using NV-centers-in-diamond optical magnetometry, New J. Phys. **20,** 043010 (2018).

[15] D. A. Broadway, B. C. Johnson, M. S. J. Barson, S. E. Lillie, N. Dontschuk, D. J. McCloskey, A. Tsai, T. Teraji, D. A. Simpson, A. Stacey, J. C. McCallum, J. E. Bradby, M. W. Doherty, L. C. L. Hollenberg, and J.-P. Tetienne, Microscopic imaging of the stress tensor in diamond using in situ quantum sensors, Nano Lett. **19,** 4543 (2019), pMID: 31150580.

[16] K. Joshi, N. Nusran, M. Tanatar, K. Cho, W. Meier, S. Bud'ko, P. Canfield, and R. Prozorov, Measuring the Lower Critical Field of Superconductors using Nitrogen-Vacancy Centers in Diamond Optical Magnetometry, Phys. Rev. Appl. **11,** 014035 (2019).

[17] Y. Schlussel, T. Lenz, D. Rohner, Y. Bar-Haim, L. Bougas, D. Groswasser, M. Kieschnick, E. Rozenberg, L. Thiel, A. Waxman, J. Meijer, P. Maletinsky, D. Budker, and R. Folman, Wide-Field Imaging of Superconductor Vortices with Electron Spins in Diamond, Phys. Rev. Appl. **10,** 034032 (2018).

[18] L. Thiel, D. Rohner, M. Ganzhorn, P. Appel, E. Neu, B. Müller, R. Kleiner, D. Koelle, and P. Maletinsky, Quantitative nanoscale vortex imaging using a cryogenic quantum magnetometer, Nat. Nanotechnol. **11,** 677 (2016).

[19] L. G. Steele, M. Lawson, M. Onyszczak, B. T. Bush, Z. Mei, A. P. Dioguardi, J. King, A. Parker, A. Pines, S. T. Weir, W. Evans, K. Visbeck, Y. K. Vohra, and N. J. Curro, Optically detected magnetic resonance of nitrogen vacancies in a diamond anvil cell using designer diamond anvils, Appl. Phys. Lett. **111,** 221903 (2017).

[20] P. Neumann, I. Jakobi, F. Dolde, C. Burk, R. Reuter, G. Waldherr, J. Honert, T. Wolf, A. Brunner, J. H. Shim, D. Suter, H. Sumiya, J. Isoya, and J. Wrachtrup, High-precision nanoscale temperature sensing using single defects in diamond, Nano Lett. **13,** 2738 (2013), pMID: 23721106.

[21] P. C. Maurer, G. Kucsko, C. Latta, L. Jiang, N. Y. Yao, S. D. Bennett, F. Pastawski, D. Hunger, N. Chisholm, M. Markham, D. J. Twitchen, J. I. Cirac, and M. D. Lukin, Room-temperature quantum bit memory exceeding one second, Science **336,** 1283 (2012).

[22] C. E. Bradley, J. Randall, M. H. Abobeih, R. C. Berrevoets, M. J. Degen, M. A. Bakker, M. Markham, D. J. Twitchen, and T. H. Taminiau, A Ten-Qubit Solid-State Spin Register with Quantum Memory up to One Minute, Phys. Rev. X **9,** 031045 (2019).

[23] A. Cooper, W. K. C. Sun, J.-C. Jaskula, and P. Cappellaro, Identification and Control of Electron-Nuclear Spin Defects in Diamond, Phys. Rev. Lett. **124,** 083602 (2020).

[24] S. Yang, Y. Wang, D. D. B. Rao, T. Hien Tran, A. S. Momenzadeh, M. Markham, D. J. Twitchen, P. Wang, W. Yang, R. Stöhr, P. Neumann, H. Kosaka, and J. Wrachtrup, High-fidelity transfer and storage of photon states in a single nuclear spin, Nat. Photonics **10,** 507 (2016).

[25] B. Hensen, H. Bernien, A. E. Dréau, A. Reiserer, N. Kalb, M. S. Blok, J. Ruitenberg, R. F. L. Vermeulen, R. N. Schouten, C. Abellán, W. Amaya, V. Pruneri, M. W. Mitchell, M. Markham, D. J. Twitchen, D. Elkouss, S. Wehner, T. H. Taminiau, and R. Hanson, Loophole-free bell inequality violation using electron spins separated by 1.3 kilometres, Nature **526,** 682 (2015).

[26] P. Neumann, N. Mizuochi, F. Rempp, P. Hemmer, H. Watanabe, S. Yamasaki, V. Jacques, T. Gaebel, F. Jelezko, and J. Wrachtrup, Multipartite entanglement among single spins in diamond, Science **320,** 1326 (2008).

[27] M. W. Doherty, N. B. Manson, P. Delaney, F. Jelezko, J. Wrachtrup, and L. C. Hollenberg, The nitrogen-vacancy colour centre in diamond, Phys. Rep. **528,** 1 (2013), the nitrogen-vacancy colour centre in diamond.

[28] Ádám Gali, Ab initio theory of the nitrogen-vacancy center in diamond, Nanophotonics **8,** 1907 (2019).

[29] M. W. Doherty, F. Dolde, H. Fedder, F. Jelezko, J. Wrachtrup, N. B. Manson, and L. C. L. Hollenberg, Theory of the ground-state spin of the NV⁻ center in diamond, Phys. Rev. B **85,** 205203 (2012).

[30] A. L. Falk, P. V. Klimov, B. B. Buckley, V. Ivády, I. A. Abrikosov, G. Calusine, W. F. Koehl, A. Gali, and D. D. Awschalom, Electrically and Mechanically Tunable Electron Spins in Silicon Carbide Color Centers, Phys. Rev. Lett. **112,** 187601 (2014).

[31] P. Udvarhelyi, V. O. Shkolnikov, A. Gali, G. Burkard, and A. Pályi, Spin-strain interaction in nitrogen-vacancy centers in diamond, Phys. Rev. B **98,** 075201 (2018).

[32] J. R. Maze, A. Gali, E. Togan, Y. Chu, A. Trifonov, E. Kaxiras, and M. D. Lukin, Properties of nitrogen-vacancy centers in diamond: The group theoretic approach, New J. Phys. **13,** 025025 (2011).

[33] M. W. Doherty, N. B. Manson, P. Delaney, and L. C. L. Hollenberg, The negatively charged nitrogen-vacancy centre in diamond: The electronic solution, New J. Phys. **13,** 025019 (2011).

[34] M. W. Doherty, V. M. Acosta, A. Jarmola, M. S. J. Barson, N. B. Manson, D. Budker, and L. C. L. Hollenberg, Temperature shifts of the resonances of the NV⁻ center in diamond, Phys. Rev. B **90,** 041201 (2014).

[35] V. Ivády, T. Simon, J. R. Maze, I. A. Abrikosov, and A. Gali, Pressure and temperature dependence of the zero-field splitting in the ground state of NV centers in diamond: A first-principles study, Phys. Rev. B **90,** 235205 (2014).

[36] M. Kobayashi and Y. Nisida, High pressure effects on photoluminescence spectra of color centers in diamond, Jpn. J. Appl. Phys. **32,** 279 (1993).

[37] B. Deng, R. Q. Zhang, and X. Q. Shi, New insight into the spin-conserving excitation of the negatively charged nitrogen-vacancy center in diamond, Sci. Rep. **4**, 5144 (2014).

[38] P. Udvarhelyi and A. Gali, Ab Initio Spin-Strain Coupling Parameters of Divacancy Qubits in Silicon Carbide, Phys. Rev. Appl. **10**, 054010 (2018).

[39] J. H. N. Loubser and J. A. van Wyk, Electron spin resonance in the study of diamond, Rep. Prog. Phys. **41**, 1201 (1978).

[40] M. Simanovskaia, K. Jensen, A. Jarmola, K. Aulenbacher, N. Manson, and D. Budker, Sidebands in optically detected magnetic resonance signals of nitrogen vacancy centers in diamond, Phys. Rev. B **87**, 224106 (2013).

[41] S. Felton, A. M. Edmonds, M. E. Newton, P. M. Martineau, D. Fisher, D. J. Twitchen, and J. M. Baker, Hyperfine interaction in the ground state of the negatively charged nitrogen vacancy center in diamond, Phys. Rev. B **79**, 075203 (2009).

[42] A. P. Nizovtsev, S. Y. Kilin, P. Neumann, F. Jelezko, and J. Wrachtrup, Quantum registers based on single NV + n ^{13}C centers in diamond: II. Spin characteristics of registers and spectra of optically detected magnetic resonance, Opt. Spectrosc. **108**, 239 (2010).

[43] N. Mizuochi, P. Neumann, F. Rempp, J. Beck, V. Jacques, P. Siyushev, K. Nakamura, D. J. Twitchen, H. Watanabe, S. Yamasaki, F. Jelezko, and J. Wrachtrup, Coherence of single spins coupled to a nuclear spin bath of varying density, Phys. Rev. B **80**, 041201 (2009).

[44] P. G. Baranov, A. A. Soltamova, D. O. Tolmachev, N. G. Romanov, R. A. Babunts, F. M. Shakhov, S. V. Kidalov, A. Y. Vul', G. V. Mamin, S. B. Orlinskii, and N. I. Silkin, Enormously high concentrations of fluorescent nitrogen-vacancy centers fabricated by sintering of detonation nanodiamonds, Small **7**, 1533 (2011).

[45] A. Gali, M. Fyta, and E. Kaxiras, Ab initio supercell calculations on nitrogen-vacancy center in diamond: Electronic structure and hyperfine tensors, Phys. Rev. B **77**, 155206 (2008).

[46] A. P. Nizovtsev, S. Y. Kilin, V. A. Pushkarchuk, A. L. Pushkarchuk, and S. A. Kuten, Quantum registers based on single NV + n ^{13}C centers in diamond: I. The spin Hamiltonian method, Opt. Spectrosc. **108**, 230 (2010).

[47] See Supplemental Material http://link.aps.org/supplemental/10.1103/PhysRevApplied.18.064042 for the theory of the ^{13}C hyperfine structure and additional data for ^{13}C hyperfine structures.

[48] X.-F. He, N. B. Manson, and P. T. H. Fisk, Paramagnetic resonance of photoexcited N-V defects in diamond. ii. hyperfine interaction with the ^{14}N nucleus, Phys. Rev. B **47**, 8816 (1993).

[49] J. Morton and K. Preston, Atomic parameters for paramagnetic resonance data, Journal of Magnetic Resonance (1969) **30**, 577 (1978).

[50] J. Xie, X. Liu, W. Zhang, S. M. Wong, X. Zhou, Y. Zhao, S. Wang, K. T. Lai, and S. K. Goh, Fragile pressure-induced magnetism in FeSe superconductors with a thickness reduction, Nano Lett. **21**, 9310 (2021), pMID: 34714653.

[51] G. J. Piermarini, S. Block, and J. Barnett, Hydrostatic limits in liquids and solids to 100 kbar, J. Appl. Phys. **44**, 5377 (1973).

[52] R. J. Angel, M. Bujak, J. Zhao, G. D. Gatta, and S. D. Jacobsen, Effective hydrostatic limits of pressure media for high-pressure crystallographic studies, J. Appl. Crystallogr. **40**, 26 (2007).

[53] N. Tateiwa and Y. Haga, Evaluations of pressure-transmitting media for cryogenic experiments with diamond anvil cell, Rev. Sci. Instrum. **80**, 123901 (2009).

[54] S. Klotz, J.-C. Chervin, P. Munsch, and G. L. Marchand, Hydrostatic limits of 11 pressure transmitting media, J. Phys. D: Appl. Phys. **42**, 075413 (2009).

[55] N. B. Manson, X.-F. He, and P. T. H. Fisk, Raman heterodyne detected electron-nuclear-double-resonance measurements of the nitrogen-vacancy center in diamond, Opt. Lett. **15**, 1094 (1990).

[56] K. Szász, T. Hornos, M. Marsman, and A. Gali, Hyperfine coupling of point defects in semiconductors by hybrid density functional calculations: The role of core spin polarization, Phys. Rev. B **88**, 075202 (2013).

[57] M. W. Swift, H. Peelaers, S. Mu, J. J. L. Morton, and C. G. Van de Walle, First-principles calculations of hyperfine interaction, binding energy, and quadrupole coupling for shallow donors in silicon, Npj Comput. Mater. **6**, 181 (2020).